AGU PUBLICATIONS

JGR

Journal of Geophysical Research: Space Physics

RESEARCH ARTICLE

10.1002/2015JA021065

Key Points:
- Ultrarelativistic electron PADs vary dynamically during storms
- Ultrarelativistic electron fluxes show slow poststorm decays
- The analyses are useful to evaluate the underlying physics

Supporting Information:
- Figures S1 and S2
- Figure S1
- Figure S2

Correspondence to:
B. Ni,
bbni@whu.edu.cn

Citation:
Ni, B., et al. (2015), Variability of the pitch angle distribution of radiation belt ultrarelativistic electrons during and following intense geomagnetic storms: Van Allen Probes observations, *J. Geophys. Res. Space Physics*, *120*, 4863–4876, doi:10.1002/2015JA021065.

Received 28 JAN 2015
Accepted 29 MAY 2015
Accepted article online 1 JUN 2015
Published online 30 JUN 2015

©2015. American Geophysical Union. All Rights Reserved.

Variability of the pitch angle distribution of radiation belt ultrarelativistic electrons during and following intense geomagnetic storms: Van Allen Probes observations

Binbin Ni[1,2], Zhengyang Zou[1], Xudong Gu[1], Chen Zhou[1], Richard M. Thorne[3], Jacob Bortnik[3], Run Shi[1], Zhengyu Zhao[1], Daniel N. Baker[4], Shrikhanth G. Kanekal[5], Harlan E. Spence[6], Geoffrey D. Reeves[7],and Xinlin Li[4]

[1]Department of Space Physics, School of Electronic Information, Wuhan University, Wuhan, China, [2]State Key Laboratory of Space Weather, Chinese Academy of Sciences, Beijing, China, [3]Department of Atmospheric and Oceanic Sciences, University of California, Los Angeles, California, USA, [4]Laboratory for Atmospheric and Space Physics, University of Colorado Boulder, Boulder, Colorado, USA, [5]NASA Goddard Space Flight Center, Greenbelt, Maryland, USA, [6]Institute for the Study of Earth, Oceans, and Space, University of New Hampshire, Durham, New Hampshire, USA, [7]Space Science and Applications Group, Los Alamos National Laboratory, Los Alamos, New Mexico, USA

Abstract Fifteen months of pitch angle resolved Van Allen Probes Relativistic Electron-Proton Telescope (REPT) measurements of differential electron flux are analyzed to investigate the characteristic variability of the pitch angle distribution of radiation belt ultrarelativistic (>2 MeV) electrons during storm conditions and during the long-term poststorm decay. By modeling the ultrarelativistic electron pitch angle distribution as $\sin^n\alpha$, where α is the equatorial pitch angle, we examine the spatiotemporal variations of the n value. The results show that, in general, n values increase with the level of geomagnetic activity. In principle, ultrarelativistic electrons respond to geomagnetic storms by becoming more peaked at 90° pitch angle with n values of 2–3 as a supportive signature of chorus acceleration outside the plasmasphere. High n values also exist inside the plasmasphere, being localized adjacent to the plasmapause and exhibiting energy dependence, which suggests a significant contribution from electromagnetic ion cyclotron (EMIC) wave scattering. During quiet periods, n values generally evolve to become small, i.e., 0–1. The slow and long-term decays of the ultrarelativistic electrons after geomagnetic storms, while prominent, produce energy and L-shell-dependent decay time scales in association with the solar and geomagnetic activity and wave-particle interaction processes. At lower L shells inside the plasmasphere, the decay time scales τ_d for electrons at REPT energies are generally larger, varying from tens of days to hundreds of days, which can be mainly attributed to the combined effect of hiss-induced pitch angle scattering and inward radial diffusion. As L shell increases to L~3.5, a narrow region exists (with a width of ~0.5 L), where the observed ultrarelativistic electrons decay fastest, possibly resulting from efficient EMIC wave scattering. As L shell continues to increase, τ_d generally becomes larger again, indicating an overall slower loss process by waves at high L shells. Our investigation based upon the $\sin^n\alpha$ function fitting and the estimate of decay time scale offers a convenient and useful means to evaluate the underlying physical processes that play a role in driving the acceleration and loss of ultrarelativistic electrons and to assess their relative contributions.

1. Introduction

The Earth's radiation belt electron dynamics is highly complex, resulting from a delicate, competitive balance between their transport, energization, and loss processes, and also shows strong dependence on a number of factors including solar wind driving condition, geomagnetic activity, electron kinetic energy, spatial location, and time [e.g., *Li et al.*, 1997; *Reeves et al.*, 1998, 2003; *Meredith et al.*, 2003; *Lee et al.*, 2013; *Ni et al.*, 2013; *Thorne et al.*, 2013a, 2013b; *Baker et al.*, 2013a, 2014a, 2014b]. It has been known that geomagnetic storms can either increase or decrease the fluxes of radiation belt relativistic electrons, with about half of all storms increasing the relativistic electron fluxes, one quarter decreasing the fluxes, and the remaining quarter producing little or no change in the fluxes [*Reeves et al.*, 2003]. However, the responsible physical processes controlling the radiation belt flux intensities in response to different geomagnetic storms are not yet fully understood. It has also been reported that corotating interaction region (CIR)-driven storms are generally of longer

duration and produce higher fluxes of radiation belt relativistic electrons compared to coronal mass ejection (CME)-driven storms, especially during the declining phase of the solar cycle when the recurring high speed streams peak [e.g., *Lam*, 2004; *Miyoshi and Kataoka*, 2005; *Borovsky and Denton*, 2006]. Unfortunately, the physics required to quantify the distinct differences in the radiation belts' responses to CIR- and CME-driven storms is not fully understood.

To better understand the potential mechanism(s) responsible for the observed electron flux variations on different spatial and temporal scales, investigation of electron pitch angle distribution (PAD) and its evolution provides a feasible and convenient means to approach the underlying physics, since electrons at different pitch angles with different energies generally behave differently when exposed to external influences. By assuming that the pitch angle distribution follows a form $\sin^n\alpha$ (where α is the particle pitch angle and n is the power law index) down to the loss cone, a number of previous studies explored the PADs of radiation belt energetic electrons, using several satellite data sets, for example, the CRRES Magnetic Electron Spectrometer [*Vampola*, 1998; *Gannon et al*., 2007; *Gu et al*., 2011] and the POLAR High Sensitivity Telescope data [*Selesnick and Kanekal*, 2009]. Based on those studies, the electron distributions can be mainly classified into three broad categories: 90°-peaked, flattop, and butterfly (see Figure 2 in *Gannon et al*. [2007]), which can be further analyzed to suggest some particular physical process. Specifically, inward radial diffusion can cause a flux increase around 90° faster than other pitch angles, thus creating an increased peak for distributions starting as 90°-peaked distributions or altering an apparent butterfly distribution at a higher L shell into a flattop and eventually into a 90°-peaked distribution at a lower L shell. Chorus wave-driven pitch angle scattering at low pitch angles and energy diffusion at higher pitch angles can also deepen the 90°-peaked distributions. However, losses to the magnetopause (magnetopause shadowing) and drift shell splitting act as a major contributor to the occurrence of butterfly distributions at higher L. In addition, scattering by plasmaspheric hiss can lead to characteristic top-hat-shaped pitch angle distributions of radiation belt energetic electrons [e.g., *Lyons et al*., 1972; *Ni et al*., 2013, 2014].

In the present study, in order to investigate in detail the PAD characteristics of radiation belt ultrarelativistic ($>$2 MeV) electrons, we adopt the new and unique data sets from the Van Allen Probes Relativistic Electron-Proton Telescope (REPT) measurements, which have become available since September 2012 and continuously provide pitch angle resolved differential electron fluxes up to ~10 MeV since the launch of the twin spacecraft. Different from previous similar studies that mainly concentrated on radiation belt electrons $<$ ~1 MeV, our study of the PADs of ultrarelativistic electrons is important especially for improved understanding of the acceleration and loss processes of these highly hazardous magnetospheric particles, which have exhibited several particular properties of their dynamic variations [e.g., *Baker et al*., 2013a, 2014a, 2014b; *Reeves et al*., 2013; *Thorne et al*., 2013a, 2013b]. In addition, the accumulation of Van Allen Probes data enables a more comprehensive investigation of the gradual, long-term decay of radiation belt ultrarelativistic electron fluxes following intense geomagnetic storms from the perspectives of both PAD evolution and the rate of electron decay.

The outline of this paper is as follows. We give the description of the instrumentation and the data availability in section 2, followed by the description of the fitting method and its goodness in section 3. Section 4 presents the results of the PADs of ultrarelativistic electrons based on the detailed analysis of 15 month Van Allen Probes REPT data. The long-term, slow decay of ultrarelativistic electron fluxes are then studied with the decay time scales quantified for three representative strong storms in section 5. We discuss the results in section 6 and summarize our conclusions in section 7.

2. Instrumentation and Data Availability

In the present study we utilize the pitch angle resolved data sets of ultrarelativistic electron fluxes measured by the REPT instrument [*Baker et al*., 2013b] on board the Van Allen Probes twin spacecraft flying near the equatorial plane [*Mauk et al*., 2013]. The REPT instrument is designed to measure the directional intensities and energy spectra of ~1–20 MeV electrons and 17–200 MeV protons at high resolution. In order to cover a wide dynamic range of electron fluxes that the spacecraft may encounter, it has an optimized geometric factor (0.2 cm^2 sr), with a circular conical field of view of 32°, to measure electron flux intensities ranging from ~10^{-2} to 10^6 el/(cm^2 s sr MeV). The instrument points perpendicular to the spin axis of the spacecraft

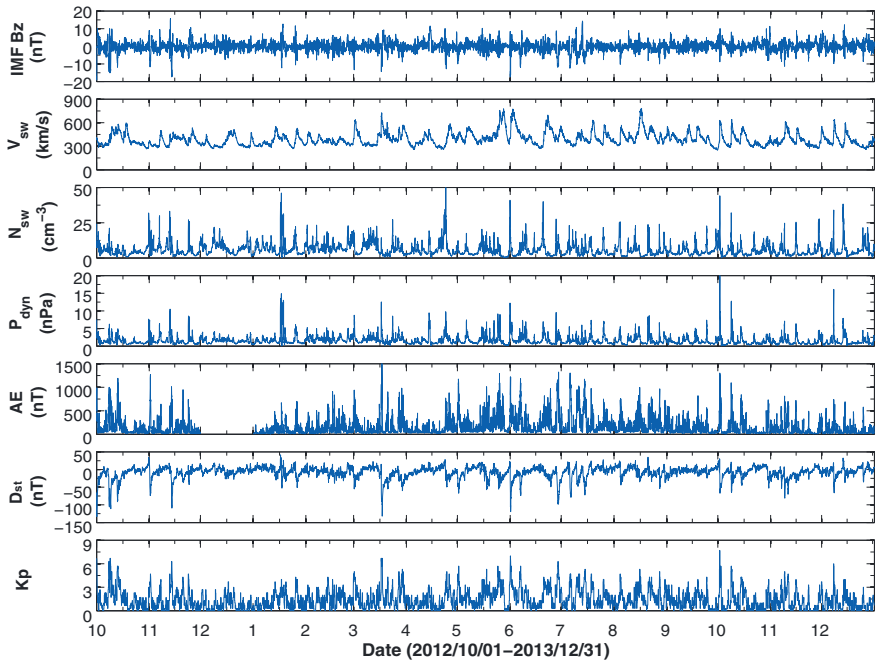

Figure 1. Temporal variations of solar wind parameters and geomagnetic indices for the considered 15 month time period from 1 October 2012 to 31 December 2013. From top to bottom: IMF B_z, solar wind speed (V_{sw}), solar wind proton density (N_{sw}), solar wind dynamic pressure (P_{dyn}), and three geomagnetic indices (*AE*, *Dst*, and *Kp*).

and thus can sample all pitch angles of particles during almost all expected magnetic field orientations. Due to its high temporal, spatial, energy, and pitch angle resolution, the REPT measurements provide a unique data set that captures the dynamical evolution of both the energy and pitch angle distribution of the highly relativistic electron population throughout the slot and outer radiation belt region [*Li et al.*, 2015]. The REPT instrument offers energy and pitch angle resolved electron measurements at 12 energy channels. The present study concentrates on the REPT observations for six channels at energies between 2.3 and 7.15 MeV.

For the 15 month time period from 1 October 2012 to 31 December 2013, Figure 1 shows, from top to bottom, the temporal variations of a number of key solar wind parameters (IMF B_z, V_{sw}, N_{sw}, and P_{dyn}) and three geomagnetic indices (*AE*, *Dst*, and *Kp*). The data are from the online OMNIWEB data service (http://omniweb.gsfc.nasa.gov/form/dx1.html) with 1 h resolution. Obvious solar wind disturbances occurred associated with the fluctuations and turnings of IMF B_z, the rapid increases of solar wind velocity, the jumps of proton density, and the solar wind dynamic pressure pulses, indicating that the solar wind activity was rather strong during the considered time span. The variations in the solar wind property during this period span the range of −19–16 nT for IMF B_z, 250–780 km/s for V_{sw}, 0–50 cm^{-3} for N_{sw}, and 0–31 nPa for P_{dyn}. Correspondingly, the *AE* index fluctuated between 0 and 1800 nT, showing the occurrence of numerous intense substorm disturbances. Together with the change of *Kp* index between 0 and 7.7, *Dst* index varied between −133 nT and 41 nT, manifesting the occurrences of geomagnetic storms at different disturbance levels.

3. Fitting Method and Its Goodness

Following previous studies [e.g., *Vampola*, 1998; *Green and Kivelson*, 2004; *Gannon et al.*, 2007; *Selesnick and Kanekal*, 2009; *Ni et al.*, 2009a, 2009b; *Gu et al.*, 2011], we assume that radiation belt electron PADs can be modeled using the following functional form

$$j = j_0 \sin^n \alpha, \tag{1}$$

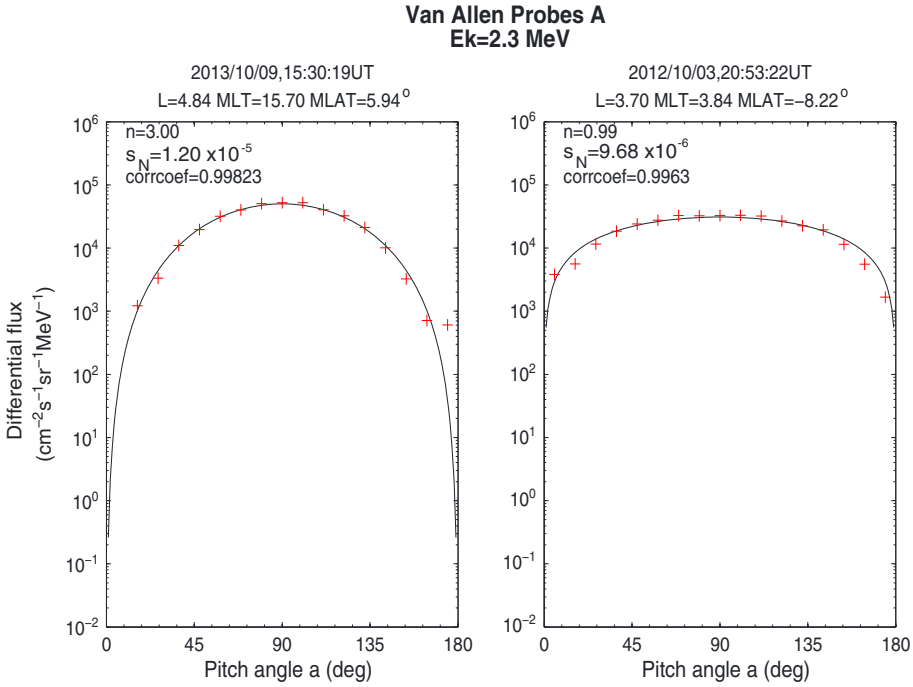

Figure 2. Two samples of REPT observed 2.3 MeV electron pitch angle distributions and sine function fitting described by equation (1).

where j is the electron differential flux, α is the pitch angle, j_0 is the electron flux at 90° pitch angle, and n is the power law index. A standard least squares fit is performed, and following *Carbary et al*. [2011], the goodness of fit is quantified by a normalized standard deviation

$$\sigma_N = \sigma/[\max(j) - \min(j)], \tag{2}$$

where σ is the usual standard deviation of the fit, max(j) is the maximal flux of the observed electron pitch angle distribution, and min(j) is the corresponding minimal flux after any zero-value flux is excluded from the data. Smaller values of normalized standard deviation σ_N represent better fits to observed pitch angle distribution by the function defined in equation (1). Specifically, $\sigma_N \leq 0.3$, $0.3 < \sigma_N \leq 0.5$, and $\sigma_N > 0.5$ indicate an excellent, rather good, and poor resemblance of observations.

We adopt the level 3 Van Allen Probes REPT data sets, which provide the pitch angle resolved differential fluxes for ultrarelativistic electrons at a number of-specific pitch angles, that is 5°, 16°, 26°, 37°, 48°, 58°, 69°, 79°, 90°, 101°, 111°, 122°, 132°, 143°, 154°, 164°, and 175°. We further assign the flux threshold value as 10^{-2} el/(cm^2 s sr MeV) [*Baker et al*., 2013b] to avoid contamination from the background noise level and remove the measurements below this value. At each time instance we also exclude the data with the number of useful points (over pitch angle) less than 3 for one energy channel so that there are enough data points for fits.

Figure 2 displays two samples of REPT observed 2.3 MeV electron pitch angle distributions and model fitting using equation (1). The annotation in each panel gives the number of nonzero fluxes, the fitted n value, the normalized standard deviation, and the correlation coefficient between observations and model results. Figure 2 (left) shows a highly 90°-peaked distribution with $n = 3$ at L = 4.8 on the afternoon side, while Figure 2 (right) shows a flatter distribution with $n = 1$ at L = 3.7 on the dawnside. Extremely small values of normalized standard deviation and ~1 correlation coefficients indicate that the sine function fits favorably reproduce the observed ultrarelativistic electron pitch angle distributions.

4. Pitch Angle Distributions of Ultrarelativistic Electrons

Based on the method described above, we first establish a robust database of REPT electron differential fluxes to investigate the PADs and the corresponding power law index (n) of the sine function fitting. Then we apply

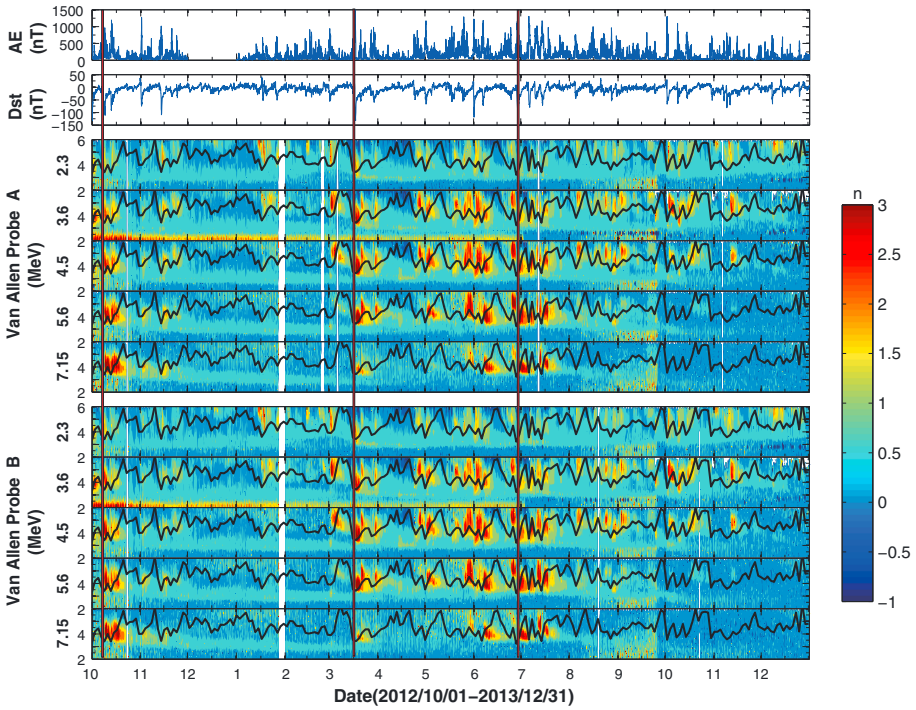

Figure 3. L shell binned and orbit-averaged n values of the $\sin^n\alpha$ function fits to radiation belt ultrarelativistic electron differential fluxes observed by the Van Allen Probes twin spacecraft during the 15 month period. The color scale specifies the fitted value of the power law index n. From top to bottom, the panels show the temporal variations of *AE*, *Dst*, and bin-averaged n values for the REPT electron energy channels at 2.3, 3.6, 4.5, 5.6, and 7.15 MeV for Van Allen Probes A and B, respectively. The overplotted thick black curve in each n value plot indicates the *Dst*-based averaged plasmapause location following the model of *O'Brien and Moldwin* [2003]. The vertical lines denote the three representative storms investigated in the study.

least squares fits of equation (1) to observed electron differential flux versus pitch angle distributions at each time point to calculate the n value for each considered REPT energy channel. Finally, we perform bin-averaging to produce a 2-D array of averaged power law index n as a function of time and L shell. Specifically, the bin size of L shell is 0.2 L for the range of L = 2–6, and the temporal bin size is an orbital period, ~ 9 h, corresponding to each spacecraft orbit. The 2-D map of bin-averaged n value is shown in Figure 3 for the indicated five REPT energy channels at 2.3, 3.6, 4.5, 5.6, and 7.15 MeV for the 15 month period. The corresponding *AE* and *Dst* indices are shown on the top two panels. The overplotted thick black trace in each flux plot indicates the *Dst*-based averaged plasmapause location following the model of *O'Brien and Moldwin* [2003].

There are a number of interesting features to point out regarding the temporal and spatial variations of the n value associated with radiation belt ultrarelativistic electron PADs:

1. The ultrarelativistic electrons responded to the majority of geomagnetic storms by becoming more peaked at 90° pitch angle with n values of 2–3. Increase of n value occurred over a broad range of L shell in association with *AE* increases and fluctuations.
2. High n values are also present just inside the plasmasphere, which are contiguous to those distributions outside and relaxed back to the prestorm (or ambient) levels with a few days. Besides being localized in L shell (i.e., adjacent to the plasmaspheric boundary), the increased n value is also energy-dependent, being much smaller for 2.3 MeV than for higher energies.
3. Obtained n values are generally relatively small, i.e., 0–1, during the quiescent periods, which is consistent with the weakness of geomagnetic activity and associated wave-particle interactions.

To check the uncertainty associated with the sine function fitting, we follow equation (2) to evaluate the normalized standard deviation σ_N as well. Scatterplots of computed σ_N values for 2.3 MeV electrons

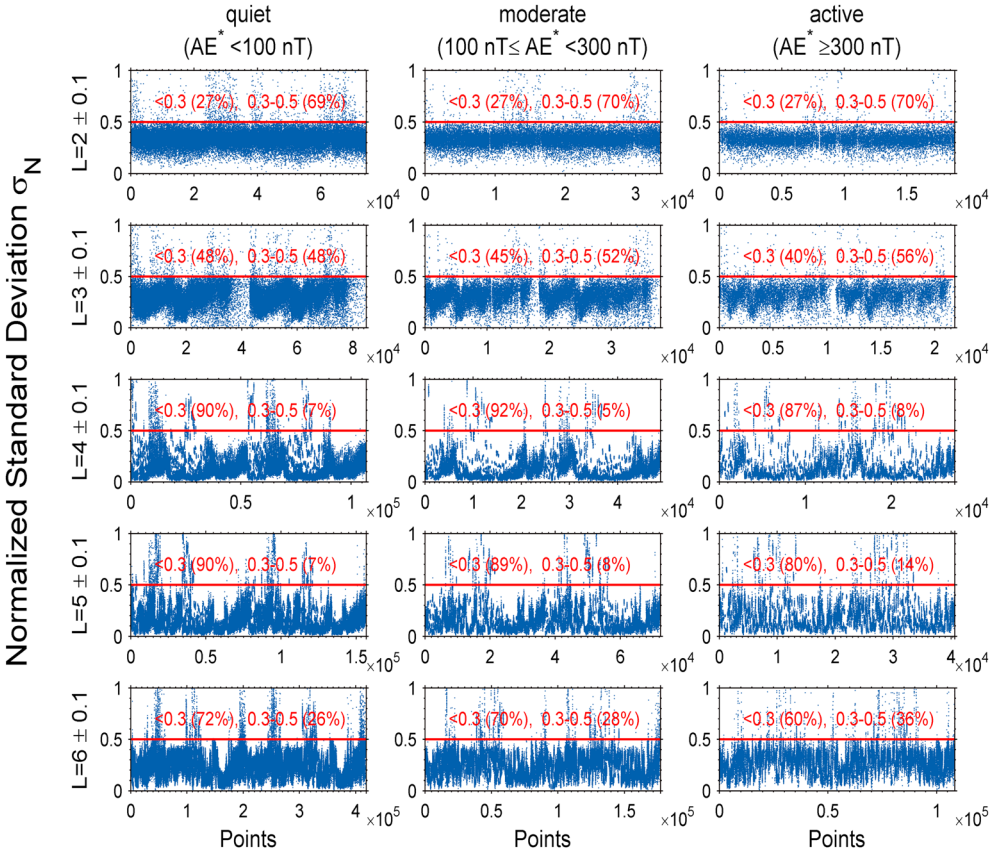

Figure 4. Scatterplots of the values of normalized standard deviation σ_N for 2.3 MeV electrons (observed by both Probes A and B) for the indicated five L shells and for the considered three geomagnetic conditions parameterized by *AE** (averaged *AE* index in the previous 1 h) during the 15 month period. The horizontal red line shows the value of $\sigma_N = 0.5$. The annotation in each panel shows the percentages of two intervals of σ_N value: $\sigma_N \leq 0.3$ and $0.3 < \sigma_N \leq 0.5$, which gives the basic information of the goodness of sine function fits.

(observed by both Probe A and B) are shown in Figure 4 as an example for the indicated five L shells and for the considered three geomagnetic conditions parameterized by *AE** (averaged *AE* index in the previous 1 h) during the 15 month period. Overall, at least 94% of fits reproduce roughly well ($\sigma_N < 0.5$) the observed profiles of REPT electron pitch angle distribution, justifying the applicability of the sine function fitting method. More specifically, sine function fitting tends to produce the best performance at the spatial extents of L = 4, 5, and 6, while the worst performance occurs at L = 2, according to the percentage of $\sigma_N \leq 0.3$. It is interesting to note that the performance of equation (1) for fits of ultrarelativistic electron pitch angle distribution seems to show little dependence on the level of geomagnetic activity. Computed σ_N values for 4.5 MeV and 7.15 MeV are shown in the supporting information, which also supports the feasibility of sine function fitting to studying REPT electron pitch angle distributions.

Figure 5 shows the (L, magnetic local time (MLT)) maps of averaged *n* value for four REPT energies under the three geomagnetic conditions (from top to bottom: quiet, moderate, and active). The bin size is 0.1 L (for L = 2–6) and 01:00 MLT (for all 24:00 MLTs). On the nightside, high *n* values occur predominantly at L ≥ 4. On the dayside, high *n* values tend to appear at higher L shells and become larger for higher energies. In general, *n* values increase with the level of geomagnetic activity, being largest during active periods regardless of electron energy. Figure 5 (bottom row) also indicates that the enhanced 90°-peaked distribution can cover a broad range of spatial locations as the geomagnetic activity remains active. As electron energy increases, smaller *n* values (denoted by the cyan to blue colors) tend to cover broader spatial regions. On the other hand, the substantial difference in *n* value between 2.3 MeV electrons and higher energy electrons suggests that there is a transition in a physical process.

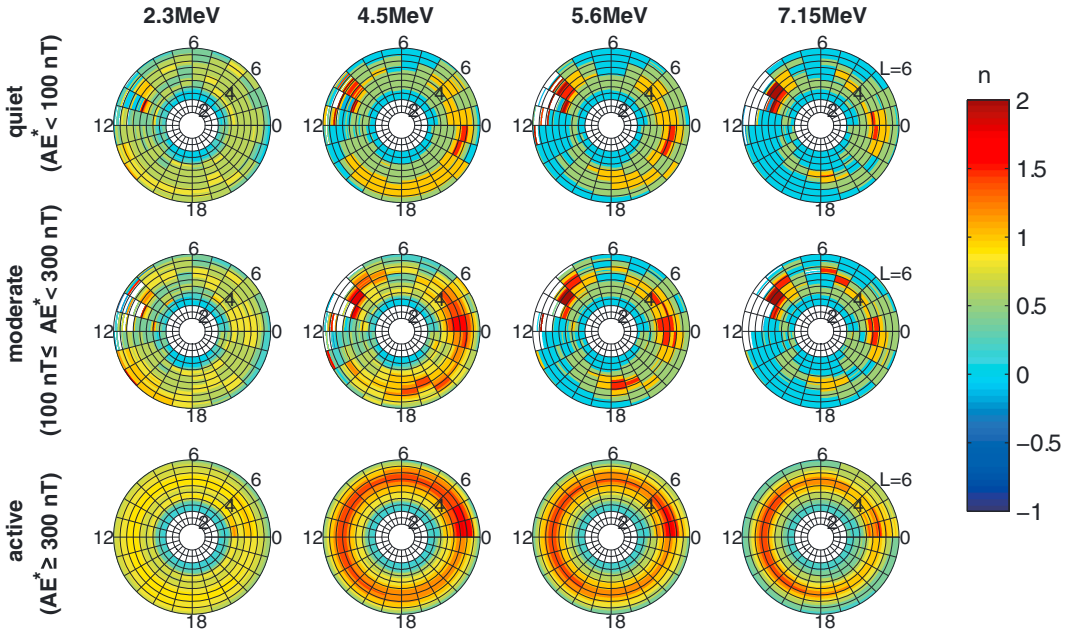

Figure 5. (L, MLT) maps of averaged *n* value for the indicated five REPT energies under the three geomagnetic conditions (from top to bottom: quiet, moderate, and active) parameterized by *AE** (averaged *AE* index in the previous 1 h) for the 15 month period.

The results shown in Figures 3 and 5 present an overall view of the temporal and spatial variations of radiation belt ultrarelativistic electron pitch angle distribution, which contains much physics. We defer the discussions on the underlying physical processes to section 6.

5. Long-Term Poststorm Decay of Ultrarelativistic Electron Fluxes

With the available n values, we can analyze the omni-directional electron flux (*J*, in the unit of 1/(cm^2 s MeV)) by integrating the pitch angle resolved electron differential fluxes (*j*, in the unit of 1/(cm^2 s sr MeV)) over pitch angle. From equation (1), we can obtain the relation $J = \int_0^{\pi} j_0 \sin^n \alpha d\alpha \int_0^{2\pi} d\varphi = 2\pi j_0 \int_0^{\pi} \sin^n \alpha d\alpha$, where φ is the azimuth angle and *n* is the power law index of the sine function with a real value. Figure 6 shows the L shell binned and orbit-averaged pitch angle integrated electron fluxes for the indicated five REPT energy channels for the 15 month period. Similar to Figure 2, the data are binned over every 0.2 L and every orbital period. The corresponding *AE* and *Dst* indices are shown on the top two panels, and the plasmapause location is overplotted as a thick black trace in each flux plot.

The dynamic characteristics of the Earth's radiation belts are apparent, showing clear evidence of associations with geomagnetic disturbances and solar wind features. Since the Probes A and B are close to each other, the flux variations observed by both spacecraft were generally very similar during the 15 month period. For simplicity, only the results for Probe A are shown. Overall, the profiles of computed pitch angle integrated ultrarelativistic electron flux show abrupt losses during the periods of high solar wind driving and geomagnetic storms, subsequent efficient local acceleration, and long-term gradual decay under low solar wind driving conditions, which is consistent with the study of *Baker et al.* [2014a] using the first year of Van Allen Probes REPT data of differential electron flux at 90° pitch angle. Radiation belt electrons at different REPT energies, however, responded distinctly to the activities of solar wind and geomagnetic disturbance. The 2.3 MeV electron population underwent energization most efficiently with largest fluxes, while a longer time was required for electron acceleration to higher energies.

There are a number of interesting storm events. For instance, the 8–9 October 2012 storm, the 17 March 2013 storm, and the 28–29 June 2013 storm, as denoted by the red vertical lines in Figure 6, occurred corresponding to the southward turning of IMF B_z and the enhancement of solar wind dynamic pressure.

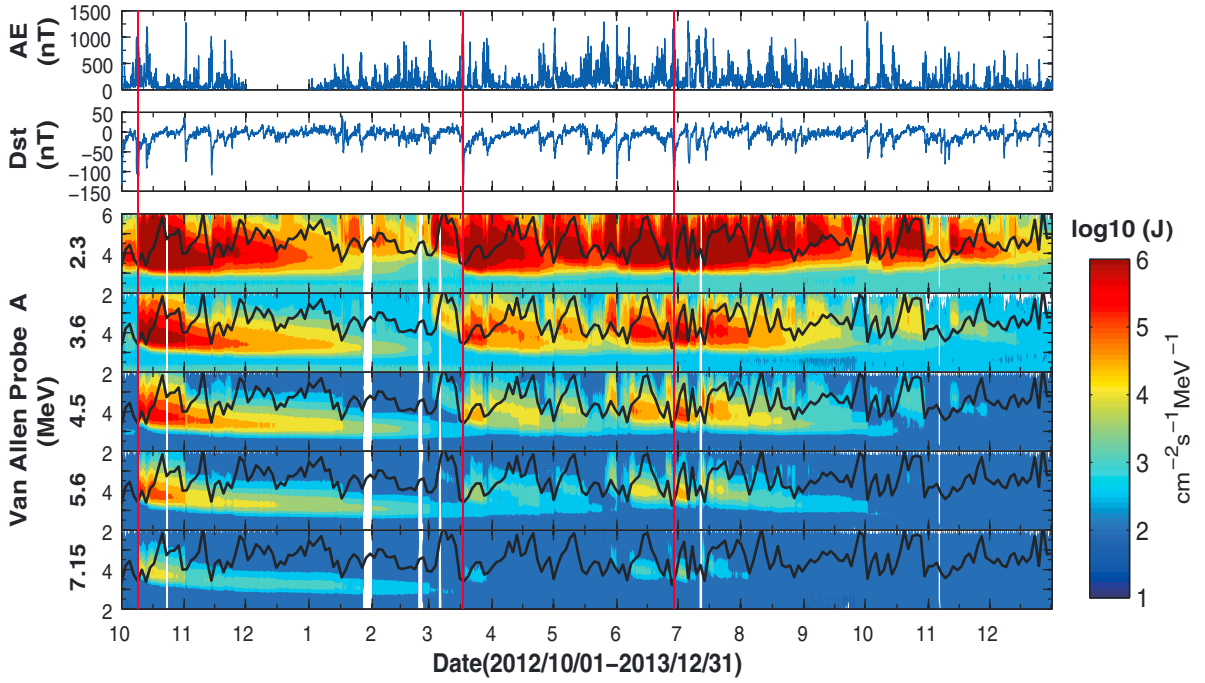

Figure 6. L shell-binned and orbit-averaged pitch angle integrated REPT electron fluxes for Van Allen Probe A during the 15 month period. The color scale specifies the logarithmic value of the flux. From top to bottom, the panels show the temporal variations of *AE*, *Dst*, and L-binned pitch angle integrated fluxes for five REPT electron energy channels with the central energy of 2.3, 3.6, 4.5, 5.6, and 7.15 MeV for Van Allen Probe A, respectively. The overplotted thick black curve in each flux plot indicates the *Dst*-based averaged plasmapause location following the model of *O'Brien and Moldwin* [2003]. The vertical lines denote the three representative storms investigated in this study. The results for Van Allen Probe B are very similar and therefore not shown.

The dynamic physics of radiation belt relativistic electrons during the first two storms, including chorus wave acceleration, ULF wave-driven radial diffusion, scattering loss due to plasmaspheric hiss and EMIC waves, and the effects of plasmaspheric erosion/recovery and magnetopause shadowing, have been extensively studied [e.g., *Reeves et al*., 2013; *Thorne et al*., 2013a; *Shprits et al*., 2013; *J. Li et al*., 2014; *W. Li et al*., 2014; *Tu et al*., 2014; *Hudson et al*., 2014; *Yu et al*., 2014; *Gkioulidou et al*., 2014; *Xiao et al*., 2014].

In the present study we are interested in the poststorm phenomena whereby the REPT ultrarelativistic electron populations frequently exhibited distinctly slow temporal decays over a broad range of L shell primarily inside the plasmapause. *Baker et al*. [2013a] reported the REPT observed evolution and slow decay of the unusual, remnant narrow ring of ultrarelativistic electrons between L = 3 and 3.5 following the September 2012 geomagnetic storm. *Thorne et al*. [2013b] quantitatively demonstrated that the long-term stability of the relativistic electron ring was associated with the rapid outward migration and maintenance of the plasmapause to distances greater than L = 4 and that pitch angle scattering by plasmaspheric hiss on time scales exceeding 10–20 days is a viable candidate to explain the temporal variation of REPT electron fluxes above 3 MeV at L~3.2.

To perform a more detailed investigation of the features concerning the slow and long-term decays of REPT ultrarelativistic electrons, here we select three representative time periods: 15 November 2012 to 15 January 2013, 20 March 2013 to 20 April 2013, and 20 July 2013 to 25 September 2013, all of which were featured with the occurrence of strong geomagnetic disturbances. The REPT observations of Van Allen Probe A are displayed in Figure 7 to show the poststorm gradual decays of electron fluxes. Probe B observations exhibited very similar profiles of electron flux evolution and thus not shown here. In general, during the intervals of intense geomagnetic activity with high *AE* and low *Dst*, the Van Allen Probes REPT fluxes were enhanced at all five energies (2.3–7. 15 MeV) for all the three L shells (L = 3, 4, and 5). Subsequent to the geomagnetically active time intervals, the outer radiation belt of ultrarelativistic electrons showed a strong tendency of flux decrease with time, which lasted longer than tens of days when the low solar wind driving condition and/or the quiet geomagnetic activity remained present. Specifically, the long-term slow decay of REPT electron fluxes was seen at L = 4 and 5 for the time periods of 15 November 2012 to

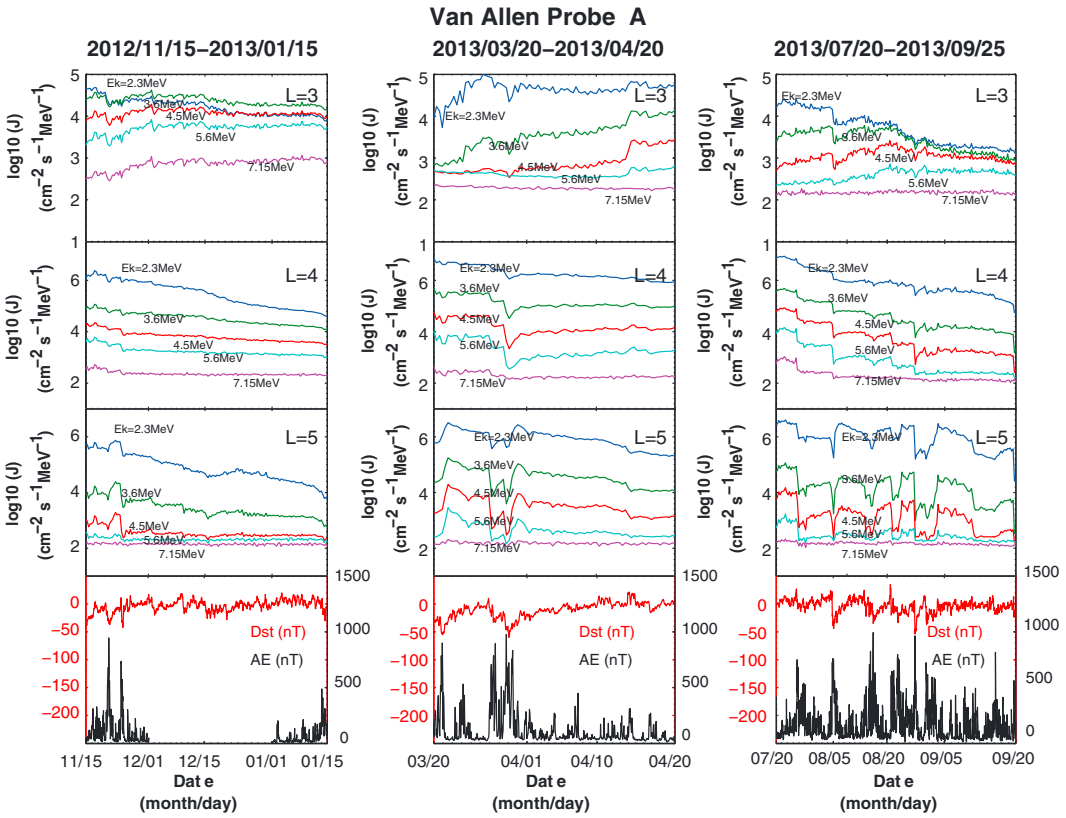

Figure 7. Pitch angle integrated REPT electron fluxes for Van Allen Probe A for the specified three time periods in association with intense geomagnetic disturbances and long-term poststorm flux decay. The panels, from left to right, show the flux evolution of five REPT electron energies (2.3, 3.6, 4.5, 5.6, and 7.15 MeV) for the three time intervals: 15 November 2012 to 15 January 2013, 20 March 2013 to 20 April 2013, and 20 July 2013 to 25 September 2013, and from top to bottom, show the results for L = 3, 4, and 5, respectively. The corresponding time series of *AE* and *Dst* are presented at the bottom row.

15 January 2013 and 20 March 2013 to 20 April 2013 and at L = 3 and 4 for the time period of 20 July 2013 to 25 September 2013. Among these three pronounced decay events, the first two corresponded well to the relatively low *AE* activity and the *Dst* recovery to the level of ~0 nT. For the third event, the geomagnetic activity remained enhanced but was considerably reduced compared to the preceding time.

While the REPT electron fluxes exhibited variations on short time scales of ~1 day, their long-term slow decreases remained prominent, which can be reasonably described with an exponentially time decaying function. We evaluate the decay time scales (τ_d) for REPT electron integrated fluxes shown in Figure 7, using the least squares exponentially decay fitting as follows,

$$J = J_0 e^{-t/\tau_d}, \tag{3}$$

where t is the time and τ_d is the characteristic decay time scale. Here the decay time scale τ_d is a quantity that describes the rate of flux drop at all pitch angles as a whole after reaching an equilibrium. For a given range of L shell, the rates of electron decay are not the same of the rates of electron loss because radial transport can either be adding or removing particles from that L shell.

Figure 8 shows the decay time scales (τ_d) as a function of L shell for the three representative long-term decay processes of the radiation belt ultrarelativistic electron fluxes. The results indicate the following:

1. Parameter τ_d varies substantially case by case. For the third period of 20 July 2013 to 25 September 2013, the geomagnetic activity remained disturbed (Figure 7) with substorm injections and the overall trend of the ultrarelativistic electron fluxes at L > 4.5 was increasing. In contrast, inside the plasmasphere the ultrarelativistic electron fluxes experienced relatively faster decrease due to

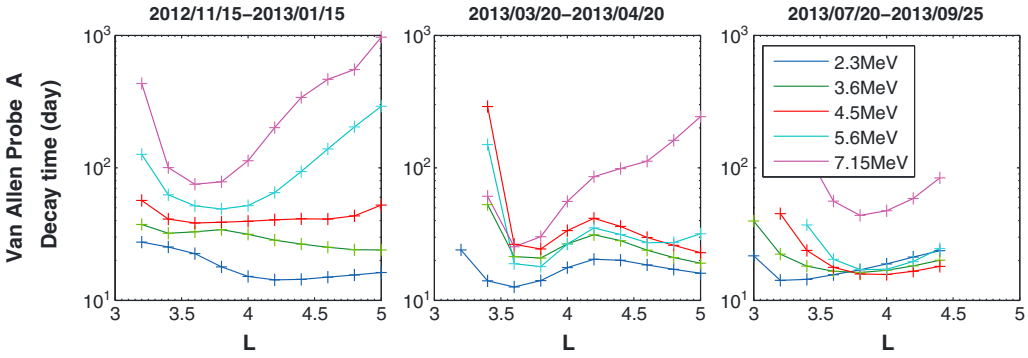

Figure 8. Poststorm decay time scales (τ_d), estimated using the least squares exponentially decay fitting described by equation (3), for REPT energy electrons as a function of L shell for the three representative long-term decay processes shown in Figure 7.

enhanced loss processes. Even for the first two periods, i.e., 15 November 2012 to 15 January 2013 and 20 March 2013 to 20 April 2013, when the geomagnetic activity was rather quiet, the features of the ultrarelativistic electron flux decay were different. The flux decay tends to be faster during the second time interval especially for higher energy electrons at L ≥ 3.5. In addition, the electron fluxes generally increased at L < ~3.5 for these two time periods.

2. Parameter τ_d is strongly energy-dependent. In principal, lower energy electrons tend to decay faster than higher-energy electrons. For the time period of 15 November 2012 to 15 January 2013, the estimated poststorm electron decay time scales are ~ 20–60 days for 2.3–4.5 MeV, ~70–300 days for 5. 6 MeV, and even higher (~100–1000 days) for 7.15 MeV. In contrast, during the time period of 20 March 2013 to 20 April 2013, the decay time scales are smaller, especially for electrons ≥3.6 MeV. Occasionally, the electron decay time can become shorter with increasing energy for the latter two periods.
3. Parameter τ_d is sensitive to the spatial location (i.e., highly L dependent). At lower L shells inside the plasmasphere, τ_d is generally larger, varying from tens of days to hundreds of days. As L shell increases to L~3.5, there tends to exist a narrow region (with an extension of ~0.5 L) where the observed REPT ultrarelativistic electrons decayed fastest. As L shell continues to increase, τ_d generally becomes larger, showing an overall slower loss process at these high L shells.

6. Discussions

While our adopted method to investigate the temporal and spatial variations of ultrarelativistic electron fluxes during and following geomagnetic storms is mature, following a number of previous studies, the accumulation of high-quality Van Allen Probes REPT pitch angle resolved flux data provides an unprecedented opportunity to comprehensively investigate the radiation belt electron dynamics at ultrarelativistic energies. The obtained results of REPT ultrarelativistic electron pitch angle distribution and flux decay time scale with respect to kinetic energy and L shell under different geomagnetic conditions offer important clues to evaluate which kinds of wave modes can play a role in the processes of electron loss and to assess their relative contributions as well. In general, *n* values increase with the level of geomagnetic activity, being obviously largest during active periods regardless of electron energy. It is further demonstrated that in principle the ultrarelativistic electrons respond to geomagnetic storms by becoming peaked at 90° pitch angle with *n* values of 2–3 as a supportive signature of chorus acceleration outside the plasmasphere [e.g., *Thorne et al.*, 2013a; *Summers et al.*, 2007; *J. Li et al.*, 2014; *W. Li et al.*, 2014].

High *n* values also exist inside the plasmasphere and relax back to the prestorm levels with a few days, quite possibly due to a combined effect of radial diffusion, pitch angle scattering, and redistribution. It is also possible that these high *n* value distribution formed outside the plasmapause and the subsequent outward expansion of the plasmasphere left them inside, which, however, is difficult to distinguish from the observations. Being localized in L shells adjacent to the plasmaspheric boundary, the peak *n* value increases with electron energy to exhibit a strong energy dependence. Such a tendency to affect higher-energy electrons more than the lower energy population is indicative of an important physical

process. On one hand, outside the plasmapause, while the local acceleration process by chorus [*Horne et al*., 2005; *Thorne et al*., 2013a] or by magnetosonic waves [*Horne et al*., 2007; *J. Li et al*., 2014; *W. Li et al*., 2014], occurs preferentially at large pitch angles to produce an increase in the *n* index, it is not expected to be so selective in energy especially at multi-MeV energies. Inside the plasmasphere or plasmaspheric plumes, hiss emissions have been long proposed as a candidate to drive scattering loss of radiation belt electrons [e.g., *Lyons et al*., 1972; *Abel and Thorne*, 1998; *Summers et al*., 2007]; however, hiss-induced pitch angle scattering, which generally takes place on a time scale of 10s–100s days and generates the top-flatted pitch angle distribution for multi-MeV electrons [e.g., *Ni et al*., 2013, 2014], is more likely to produce lower *n* values and thus cannot explain the rapid increase of *n* value. On the other hand, EMIC waves are known to preferentially resonate with >2 MeV electrons in the Earth's magnetosphere [*Summers and Thorne*, 2003; *Meredith et al*., 2003; *Chen et al*., 2013; *Usanova et al*., 2014], over a limited range of pitch angles, which exclude the region around 90°. We consequently suggest that EMIC wave scattering could be an important contributor accounting for the high *n* values found inside the plasmapause. The reason is twofold: (1) EMIC waves characteristically scatter the resonant electrons at lower pitch angles causing loss to the atmosphere but leave the population at high pitch angles unaffected [*Usanova et al*., 2014], which can explain the increase in *n* value and (2) EMIC wave scattering can progressively extend to larger pitch angles when electron energy increases, thereby producing a more 90°-peaked distribution (i.e., higher *n* value) at higher energies, consistent with the results shown in Figure 3. In addition, as shown in Figure 5, the substantial difference in *n* value between 2.3 MeV electrons and higher-energy electrons suggests that there is a transition in a physical process, which may be associated with the minimum resonant electron energies of EMIC waves at ~2 MeV [e.g., *Summers and Thorne*, 2003; *Meredith et al*., 2003; *Chen et al*., 2013]. The potential importance of EMIC wave scattering to the Van Allen Probes electron dynamics at the REPT energies has been recently analyzed by *Ma et al*. [2015], who performed a detailed 3-D diffusion simulation to find that pitch angle scattering by EMIC waves should be incorporated to better understand the quiet time evolution of relativistic electron fluxes. The L shell and energy-dependent profile of the PAD *n* index reported here for the REPT energy channels strongly supports the significant role that EMIC wave plays in controlling the ultrarelativistic electron dynamics, which, however, is beyond the scope of the present study and will be carefully addressed in a future publication.

During quiet periods, *n* values are generally small around 0–1, suggesting that the pitch angle distributions at the REPT energies are relatively stable and wave-induced diffusion processes are insignificant. Since the REPT energy channels are around the background level in the slot region where ultrarelativistic electrons are hard to penetrate [*Baker et al*., 2014b], the obtained slot region ultrarelativistic electron distributions require further verification.

During the intervals of intense geomagnetic activity (reflected as high *AE* and low *Dst*), the Van Allen Probes REPT fluxes show enhancements at all ultrarelativistic electron energies in the radiation belts. Subsequent to the geomagnetically active time intervals, the outer radiation belt of ultrarelativistic electrons frequently exhibit a strong tendency of flux decrease with time, which can last even longer than tens of days when the low solar wind driving condition and/or the quiet geomagnetic activity remains present. While the long-term slow decreases are prominent, the estimated time scales for the gradual poststorm decay vary substantially case by case, relying on the solar and geomagnetic activity and the associated wave-particle interaction processes. At lower L shells inside the plasmasphere, the decay time scales τ_d for electrons at REPT energies are generally larger, varying from tens of days to hundreds of days, which could be mainly attributed to the combined effects of hiss induced pitch angle scattering and inward radial diffusion. As L shell increases to L~3.5, in principle the observed REPT ultrarelativistic electrons decay fastest. Since this region is roughly coincident with the common spatial location of the plasmapause, a high-density plasmaspheric boundary layer ideal for the growth of EMIC waves [e.g., *Chen et al*., 2009], it is natural to connect the faster ultrarelativistic electron flux decay at this region to EMIC wave scattering loss at rates more efficient than hiss scattering. As L shell continues to increase, τ_d generally increases, indicating an overall slower loss process by waves at these high L shells. In addition, the occasions that τ_d decreases with increasing energy suggest a delicate competition between the electron transport, acceleration, and loss processes, which, however, is outside the scope of this study.

Overall, evaluations of poststorm ultrarelativistic electron decay time scales (Figures 6–8) provide results consistent with the information obtained from the power law index (n) profiles of the electron PAD at the REPT energies (Figures 3 and 5). While plasmaspheric hiss has been long proposed as a major driver of the loss and decay of radiation belt relativistic electrons inside the plasmasphere, our results support the scenario that EMIC wave scattering also play a significant role in causing the scattering loss of ultrarelativistic electrons especially during geomagnetically quiet periods after intense storm and substorm activities. Recently, *Ripoll et al*. [2014] used several years of HEO3 measurements to investigate the long decays of radiation belt electrons in the vicinity of the slot region and to quantify the relative contributions from various whistler mode waves. For the ultrarelativistic energies of our interest, their results (Figure 5 in *Ripoll et al*. [2014]) presented mean lifetimes of ~20–50 days at L = 3–4 for >3 MeV electrons with a minimum at L~3.5, quantitatively consistent with our results especially for the third storm period.

7. Conclusions

In the present study, we have analyzed a 15 month period, using the pitch angle resolved Van Allen Probes REPT measurements of differential electron flux to investigate in detail the characteristics of the pitch angle distribution (PAD) of radiation belt ultrarelativistic (>2 MeV) electrons. By assuming that the ultrarelativistic electron pitch angle distribution can be reasonably described by the function $\sin^n\alpha$, we have fitted the observed distributions and examined the spatiotemporal variations of the n value. The major conclusions are summarized as follows:

1. In principle, n values increase with the level of geomagnetic activity. Ultrarelativistic electrons respond actively to geomagnetic storms by becoming more peaked at 90° pitch angle with n values of 2–3 as a supportive signature of chorus acceleration outside the plasmasphere.
2. High n values also exist inside the plasmasphere, being localized adjacent to the plasmapause and exhibiting energy dependence, which suggests a significant contribution from EMIC wave scattering.
3. During quiet periods, n values generally evolve to become small, i.e., 0–1, inferring that the pitch angle distributions at the REPT energies are relatively stable and wave-induced diffusion processes are insignificant.
4. The slow and long-term decays of the ultrarelativistic electrons after geomagnetic storms, while prominent, produce energy and L shell-dependent decay time scales. At lower L shells inside the plasmasphere, the decay time scales τ_d for electrons at REPT energies vary from tens of days to hundreds of days, which can be mainly attributed to the combined effect of hiss-induced pitch angle scattering and inward radial diffusion. As L shell increases to L~3.5, the observed ultrarelativistic electrons decay fastest, possibly resulting from efficient EMIC wave scattering. As L shell continues to increase, τ_d generally increases again, indicating an overall slower loss process by waves at high L shells.

In conclusion, the temporal and spatial variations of n value (the power law index of $\sin^n\alpha$ form distribution) and the profiles of the flux decay time scale with respect to kinetic energy and L shell derived for ultrarelativistic electrons can provide important information to evaluate the underlying physical processes that play a role in driving the acceleration and loss of highly relativistic electrons and to assess their relative contributions. While quantitative analyses in terms of numerical simulations are required to quantitatively and reliably identify the various drivers responsible for the dynamical variations of radiation belt ultrarelativistic electrons, our performed investigation based upon the $\sin^n\alpha$ function fitting and the estimates of decay time scale offers a convenient and useful means to quickly understand the complex behaviors of the highly hazardous, highly relativistic electron population, which has exhibited several particular properties of their dynamic variations.

Acknowledgments

This work was supported by the NSFC grants 41204120 and 41474141, the Fundamental Research Funds for the Central Universities grant 2042014kf0251, and the Project Supported by the Specialized Research Fund for State Key Laboratories. This work was also supported by JHU/APL contracts 967399 and 921647 under NASA's prime contract NAS5-01072. The analysis at UCLA was supported by the ECT sub-award 13-041 and NASA grant NNX11AR64G. Van Allen Probes REPT data were obtained from http://www.rbsp-ect.lanl.gov/science/DataDirectories.php.

M. Balikhin thanks three anonymous reviewers for their assistance in evaluating this paper.

References

Abel, B., and R. M. Thorne (1998), Electron scattering loss in Earth's inner magnetosphere: 2. Sensitivity to model parameters, *J. Geophys. Res.*, *103*(A2), 2397–2407, doi:10.1029/97JA02920.

Baker, D. N., et al. (2013a), A long-lived relativistic electron storage ring embedded in Earth's outer Van Allen belt, *Science*, *340*(6129), 186–190.

Baker, D. N., et al. (2013b), The Relativistic Electron-Proton Telescope (REPT) instrument on board the Radiation Belt Storm Probes (RBSP) spacecraft: Characterization of Earth's radiation belt high-energy particle populations, *Space Sci. Rev.*, *179*, 337–381, doi:10.1007/s11214-012-9950-9.

Baker, D. N., et al. (2014a), Gradual diffusion and punctuated phase space density enhancements of highly relativistic electrons: Van Allen Probes observations, *Geophys. Res. Lett.*, *41*, 1351–1358, doi:10.1002/2013GL058942.
Baker, D. N., et al. (2014b), An impenetrable barrier to ultrarelativistic electrons in the Van Allen radiation belts, *Nature*, *515*(7528), 186–190, doi:10.1038/nature13956.
Borovsky, J. E., and M. H. Denton (2006), Differences between CME-driven storms and CIR-driven storms, *J. Geophys. Res.*, *111*, A07S08, doi:10.1029/2005JA011447.
Carbary, J. F., D. G. Mitchell, C. Paranicas, E. C. Roelof, S. M. Krimigis, N. Krupp, K. Khurana, and M. Dougherty (2011), Pitch angle distributions of energetic electrons at Saturn, *J. Geophys. Res.*, *116*, A01216, doi:10.1029/2010JA015987.
Chen, L., R. M. Thorne, and R. B. Horne (2009), Simulation of EMIC wave excitation in a model magnetosphere including structured high-density plumes, *J. Geophys. Res.*, *114*, A07221, doi:10.1029/2009JA014204.
Chen, L., R. M. Thorne, Y. Y. Shprits, and B. Ni (2013), An improved dispersion relation for parallel propagating electromagnetic waves in warm plasmas: Application to electron scattering, *J. Geophys. Res. Space Physics*, *118*, 2185–2195, doi:10.1002/jgra.50260.
Gannon, J. L., X. Li, and D. Heynderickx (2007), Pitch angle distribution analysis of radiation belt electrons based on Combined Release and Radiation Effects Satellite Medium Electrons A data, *J. Geophys. Res.*, *112*, A05212, doi:10.1029/2005JA011565.
Gkioulidou, M., A. Y. Ukhorskiy, D. G. Mitchell, T. Sotirelis, B. H. Mauk, and L. J. Lanzerotti (2014), The role of small-scale ion injections in the buildup of Earth's ring current pressure: Van Allen Probes observations of the 17 March 2013 storm, *J. Geophys. Res. Space Physics*, *119*, 7327–7342, doi:10.1002/2014JA020096.
Green, J. C., and M. G. Kivelson (2004), Relativistic electrons in the outer radiation belt: Differentiating between acceleration mechanisms, *J. Geophys. Res.*, *109*, A03213, doi:10.1029/2003JA010153.
Gu, X., Z. Zhao, B. Ni, Y. Shprits, and C. Zhou (2011), Statistical analysis of pitch angle distribution of radiation belt energetic electrons near the geostationary orbit: CRRES observations, *J. Geophys. Res.*, *116*, A01208, doi:10.1029/2010JA016052.
Horne, R. B., R. M. Thorne, S. A. Glauert, J. M. Albert, N. P. Meredith, and R. R. Anderson (2005), Timescale for radiation belt electron acceleration by whistler mode chorus waves, *J. Geophys. Res.*, *110*, A03225, doi:10.1029/2004JA010811.
Horne, R. B., R. M. Thorne, S. A. Glauert, N. P. Meredith, D. Pokhotelov, and O. Santolík (2007), Electron acceleration in the Van Allen radiation belts by fast magnetosonic waves, *Geophys. Res. Lett.*, *34*, L17107, doi:10.1029/2007GL030267.
Hudson, M. K., D. N. Baker, J. Goldstein, B. T. Kress, J. Paral, F. R. Toffoletto, and M. Wiltberger (2014), Simulated magnetopause losses and Van Allen Probe flux dropouts, *Geophys. Res. Lett.*, *41*, 1113–1118, doi:10.1002/2014GL059222.
Lam, H.-L. (2004), On the prediction of relativistic electron fluence based on its relationship with geomagnetic activity over a solar cycle, *J. Atmos. Sol. Terr. Phys.*, *66*, 1703.
Lee, D.-Y., D.-K. Shin, J.-H. Kim, J.-H. Cho, K.-C. Kim, J. A. Hwang, D. L. Turner, T. K. Kim, and M.-Y. Park (2013), Long-term loss and re-formation of the outer radiation belt, *J. Geophys. Res. Space Physics*, *118*, 3297–3313, doi:10.1002/jgra.50357.
Li, J., et al. (2014), Interactions between magnetosonic waves and radiation belt electrons: Comparisons of quasi-linear calculations with test particle simulations, *Geophys. Res. Lett.*, *41*, 4828–4834, doi:10.1002/2014GL060461.
Li, W., et al. (2014), Radiation belt electron acceleration by chorus waves during the 17 March 2013 storm, *J. Geophys. Res. Space Physics*, *119*, 4681–4693, doi:10.1002/2014JA019945.
Li, X., D. N. Baker, M. Temerin, T. E. Cayton, G. D. Reeves, R. A. Christiansen, J. B. Blake, M. D. Looper, R. Nakamura, and S. G. Kanekal (1997), Multisatellite observations of the outer zone electron variation during the November 3–4, 1993, magnetic storm, *J. Geophys. Res.*, *102*, 14,123–14,140, doi:10.1029/97JA01101.
Li, X., R. S. Selesnick, D. N. Baker, A. N. Jaynes, S. G. Kanekal, Q. Schiller, L. Blum, J. Fennell, and J. B. Blake (2015), Upper limit on the inner radiation belt MeV electron intensity, *J. Geophys. Res. Space Physics*, *120*, 1215–1228, doi:10.1002/2014JA020777.
Lyons, L. R., R. M. Thorne, and C. F. Kennel (1972), Pitch-angle diffusion of radiation belt electrons within the plasmasphere, *J. Geophys. Res.*, *77*, 3455–3474, doi:10.1029/JA077i019p03455.
Ma, Q., et al. (2015), Modeling inward diffusion and slow decay of energetic electrons in the Earth's outer radiation belt, *Geophys. Res. Lett.*, *42*, 987–995, doi:10.1002/2014GL062977.
Mauk, B. H., N. J. Fox, S. G. Kanekal, R. L. Kessel, D. G. Sibeck, and A. Ukhorskiy (2013), Science objectives and rationale for the Radiation Belt Storm Probes mission, *Space Sci. Rev.*, *179*, 3–27, doi:10.1007/s11214-012-9908-y.
Meredith, N. P., R. M. Thorne, R. B. Horne, D. Summers, B. J. Fraser, and R. R. Anderson (2003), Statistical analysis of relativistic electron energies for cyclotron resonance with EMIC waves observed on CRRES, *J. Geophys. Res.*, *108*(A6), 1250, doi:10.1029/2002JA009700.
Miyoshi, Y., and R. Kataoka (2005), Ring current ions and radiation belt electrons during geomagnetic storms driven by coronal mass ejections and corotating interaction regions, *Geophys. Res. Lett.*, *32*, L21105, doi:10.1029/2005GL024590.
Ni, B., Y. Shprits, T. Nagai, R. M. Thorne, Y. Chen, D. Kondrashov, and H.-J. Kim (2009a), Reanalyses of the radiation belt electron phase space density using nearly equatorial CRRES and polar-orbiting Akebono satellite observations, *J. Geophys. Res.*, *114*, A05208, doi:10.1029/2008JA013933.
Ni, B., Y. Shprits, R. M. Thorne, R. Friedel, and T. Nagai (2009b), Reanalysis of relativistic radiation belt electron phase space density using multisatellite observations: Sensitivity to empirical magnetic field models, *J. Geophys. Res.*, *114*, A12208, doi:10.1029/2009JA014438.
Ni, B., J. Bortnik, R. M. Thorne, Q. Ma, and L. Chen (2013), Resonant scattering and resultant pitch angle evolution of relativistic electrons by plasmaspheric hiss, *J. Geophys. Res. Space Physics*, *118*, 7740–7751, doi:10.1002/2013JA019260.
Ni, B., et al. (2014), Resonant scattering of energetic electrons by unusual low frequency hiss, *Geophys. Res. Lett.*, *41*, 1854–1861, doi:10.1002/2014GL059389.
O'Brien, T. P., and M. B. Moldwin (2003), Empirical plasmapause models from magnetic indices, *Geophys. Res. Lett.*, *30*(4), 1152, doi:10.1029/2002GL016007.
Reeves, G. D., D. N. Baker, R. D. Belian, J. B. Blake, T. E. Cayton, J. F. Fennell, R. H. W. Friedel, M. M. Meier, R. S. Selesnick, and H. E. Spence (1998), The global response of relativistic radiation belt electrons to the January 1997 magnetic cloud, *Geophys. Res. Lett.*, *25*, 3265–3268, doi:10.1029/98GL02509.
Reeves, G. D., K. L. McAdams, R. H. W. Friedel, and T. P. O'Brien (2003), Acceleration and loss of relativistic electrons during geomagnetic storms, *Geophys. Res. Lett.*, *30*(10), 1529, doi:10.1029/2002GL016513.
Reeves, G. D., et al. (2013), Electron acceleration in the heart of the Van Allen radiation belts, *Science*, *341*(6149), 991–994, doi:10.1126/science.1237743.
Ripoll, J. F., Y. Chen, J. Fennell, and R. Friedel (2014), On long decays of electrons in the vicinity of the slot region observed by HEO3, *J. Geophys. Res. Space Physics*, *120*, 460–478, doi:10.1002/2014JA020449.
Selesnick, R. S., and S. G. Kanekal (2009), Variability of the total radiation belt electron content, *J. Geophys. Res.*, *114*, A02203, doi:10.1029/2008JA013432.

Shprits, Y. Y., D. Subbotin, A. Drozdov, M. E. Usanova, A. Kellerman, K. Orlova, D. N. Baker, D. L. Turner, and K.-C. Kim (2013), Unusual stable trapping of the ultrarelativistic electrons in the Van Allen radiation belts, *Nat. Phys.*, *9*, 699–703, doi:10.1038/nphys2760.

Summers, D., and R. M. Thorne (2003), Relativistic electron pitch-angle scattering by electromagnetic ion cyclotron waves during geomagnetic storms, *J. Geophys. Res.*, *108*(A4), 1143, doi:10.1029/2002JA009489.

Summers, D., B. Ni, and N. P. Meredith (2007), Timescales for radiation belt electron acceleration and loss due to resonant wave-particle interactions: 2. Evaluation for VLF chorus, ELF hiss, and electromagnetic ion cyclotron waves, *J. Geophys. Res.*, *112*, A04207, doi:10.1029/2006JA011993.

Thorne, R. M., W. Li, B. Ni, Q. Ma, J. Bortnik, L. Chen, and S. G. Kanekal (2013a), Rapid local acceleration of relativistic radiation-belt electrons by magnetospheric chorus, *Nature*, *504*(7480), 411–414, doi:10.1038/nature12889.

Thorne, R. M., et al. (2013b), Evolution and slow decay of an unusual narrow ring of relativistic electrons near L ~ 3.2 following the September 2012 magnetic storm, *Geophys. Res. Lett.*, *40*, 3507–3511, doi:10.1002/grl.50627.

Tu, W., G. S. Cunningham, Y. Chen, S. K. Morley, G. D. Reeves, J. B. Blake, and H. Spence (2014), Event-specific chorus wave and electron seed population models in DREAM3D using the Van Allen Probes, *Geophys. Res. Lett.*, *41*, 1359–1366, doi:10.1002/2013GL058819.

Usanova, M. E., F. Darrouzet, I. R. Mann, and J. Bortnik (2013), Statistical analysis of EMIC waves in plasmaspheric plumes from Cluster observations, *J. Geophys. Res. Space Physics*, *118*, 4946–4951, doi:10.1002/jgra.50464.

Usanova, M. E., et al. (2014), Effect of EMIC waves on relativistic and ultrarelativistic electron populations: Ground-based and Van Allen Probes observations, *Geophys. Res. Lett.*, *41*, 1375–1381, doi:10.1002/2013GL059024.

Vampola, A. L. (1998), Outer zone energetic electron environment update, in *Conference on the High Energy Radiation Background in Space*, pp. 128–136, IEEE Press, Piscataway, N. J.

Xiao, F., et al. (2014), Chorus acceleration of radiation belt relativistic electrons during March 2013 geomagnetic storm, *J. Geophys. Res. Space Physics*, *119*, 3325–3332, doi:10.1002/2014JA019822.

Yu, Y., V. Jordanova, D. Welling, B. Larsen, S. G. Claudepierre, and C. Kletzing (2014), The role of ring current particle injections: Global simulations and Van Allen Probes observations during 17 March 2013 storm, *Geophys. Res. Lett.*, *41*, 1126–1132, doi:10.1002/2014GL059322.